



PB98-146186

DOT/FAA/AR-95/111

Office of Aviation Research
Washington, D.C. 20591

Stress-Intensity Factors for Elliptical Cracks Emanating From Countersunk Rivet Holes

April 1998

Final Report

This document is available to the U.S. public
through the National Technical Information
Service (NTIS), Springfield, Virginia 22161.



**U.S. Department of Transportation
Federal Aviation Administration**

REPRODUCED BY: **NTIS**
U.S. Department of Commerce
National Technical Information Service
Springfield, Virginia 22161

NOTICE

This document is disseminated under the sponsorship of the U.S. Department of Transportation in the interest of information exchange. The United States Government assumes no liability for the contents or use thereof. The United States Government does not endorse products or manufacturers. Trade or manufacturer's names appear herein solely because they are considered essential to the objective of this report.

PROTECTED UNDER INTERNATIONAL COPYRIGHT
ALL RIGHTS RESERVED.
NATIONAL TECHNICAL INFORMATION SERVICE
U.S. DEPARTMENT OF COMMERCE

Reproduced from
best available copy.



1. Report No. DOT/FAA/AR-95/111		2. Government Accession No.		3. Recipient's Catalog No.	
4. Title and Subtitle STRESS-INTENSITY FACTORS FOR ELLIPTICAL CRACKS EMANATING FROM COUNTERSUNK RIVET HOLES				5. Report Date April 1998	
				6. Performing Organization Code	
7. Author(s) M. Gosz, University of New Hampshire, and B. Moran, Northwestern University				8. Performing Organization Report No.	
9. Performing Organization Name and Address Department of Mechanical Engineering University of New Hampshire Durham, NH 03824 Department of Civil Engineering Northwestern University Evanston, IL 60208				10. Work Unit No. (TRAIS)	
				11. Contract or Grant No.	
12. Sponsoring Agency Name and Address U.S. Department of Transportation Federal Aviation Administration Office of Aviation Research Washington, DC 20591				13. Type of Report and Period Covered Final Report	
				14. Sponsoring Agency Code AAR-433	
15. Supplementary Notes The Federal Aviation Administration William J. Hughes technical manager is John Bakuckas, AAR-433.					
16. Abstract Small cracks developing from rivet holes in lap joints of fuselage structure have been an issue of concern over the past decade. Stress-intensity factor solutions required to assess the structural integrity of such configurations are lacking. To address this need, the domain integral method was used in this research to obtain the mode I, normalized stress-intensity factor distributions for cracks emanating from a centrally located countersunk rivet hole in a square plate subjected to remote tension. Particular attention was focused on short cracks with an elliptical shape that have not propagated through the thickness. For these short cracks, the normalized stress-intensity factor distribution depended on the shape and size of the crack. Analysis was also conducted on long through-the-thickness cracks with a straight front for which the normalized stress-intensity factors were uniform.					
17. Key Words Domain integral, Finite element method, Mode I, Tensile loading			18. Distribution Statement Document is available to the public through the National Technical Information Service (NTIS), Springfield, Virginia 22161		
19. Security Classif. (of this report) Unclassified		20. Security Classif. (of this page) Unclassified		21. No. of Pages 30	
				22. Price	

ACKNOWLEDGMENTS

The research support of the Federal Aviation Administration through the Center for Aviation Systems Reliability at Iowa State University is gratefully acknowledged.

TABLE OF CONTENTS

	Page
EXECUTIVE SUMMARY	ix
1. INTRODUCTION	1
2. PROBLEM FORMULATION	2
3. DOMAIN INTEGRAL METHOD	4
4. NUMERICAL RESULTS	10
5. SUMMARY AND CONCLUDING REMARKS	21
6. REFERENCES	22

LIST OF FIGURES

Figure		Page
1	Specimen Geometry ($W/H=1.0$, $W/R=9.6$, $\sigma_0=1$ MPa)	2
2	Specimen Geometry ($h/t=0.2$, $\phi=50^\circ$, $R/t=1.954$)	3
3	The Three Crack Growth Regions I, II, and III	3
4	A Point s Lying on a Curved Crack Front	4
5	The Domain V Enclosed by the Tubular Surfaces S_t and Γ_t	5
6	Cross Section of a Finite Element Mesh Perpendicular to the Crack Plane Passing Through Node M	6
7	Cross Section of a Finite Element Mesh Parallel to the Crack Plane and Passing Through Node M	7
8	The Finite Element Mesh for the Case of an Elliptical Crack Located in Region I	8
9	A Magnification of the Mesh Near the Intersection Between the Countersunk and Straight Shank Portion of the Rivet Hole	9
10	The Finite Element Domains Along an Elliptical Crack Front	9
11	Boundary Correction Factors F Versus Physical Angle θ for Elliptical Cracks Located in Region I ($a/c = 0.4$, $c/h = 0.4, 0.6$, and 0.8)	11
12	Boundary Correction Factors F Versus Physical Angle θ for Elliptical Cracks Located in Region I ($a/c = 0.8$, $c/h = 0.2, 0.4, 0.6$, and 0.8)	11
13	Boundary Correction Factors F Versus Physical Angle θ for Elliptical Cracks Located in Region I ($a/c = 1.0$, $c/h = 0.2, 0.4, 0.6$, and 0.8)	12
14	Boundary Correction Factors F Versus Physical Angle θ for Elliptical Cracks Located in Region II ($a/c = 0.4$, $a/t = 0.16, 0.32, 0.5, 0.7$, and 0.9)	13
15	Boundary Correction Factors F Versus Physical Angle θ for Elliptical Cracks Located in Region II ($a/c = 0.8$, $a/t = 0.32, 0.5, 0.7$, and 0.9)	13
16	Normalized Mode I Stress-Intensity Factors Along Straight Crack Fronts in Region III ($a/t = 1.1, 1.2, 1.4, 1.6$, and 2.0)	14

LIST OF TABLES

Table		Page
1	Tabulated Values of the Boundary Correction Factors F Versus Physical Angle θ for Elliptical Cracks Located in Region I ($a/c = 0.4$, $c/h = 0.4, 0.6$, and 0.8)	15
2	Tabulated Values of the Boundary Correction Factors F Versus Physical Angle θ for Elliptical Cracks Located in Region I ($a/c = 0.8$, $c/h = 0.2, 0.4, 0.6$, and 0.8)	16
3	Tabulated Values of the Boundary Correction Factors F Versus Physical Angle θ for Elliptical Cracks Located in Region I ($a/c = 1.0$, $c/h = 0.2, 0.4, 0.6$, and 0.8)	17
4	Tabulated Values of the Boundary Correction Factors F Versus Physical Angle θ for Elliptical Cracks Located in Region II ($a/c = 0.8$, $a/t = 0.16, 0.32, 0.5, 0.7$, and 0.9)	18
5	Tabulated Values of the Boundary Correction Factors F Versus Physical Angle θ for Elliptical Cracks Located in Region II ($a/c = 0.8$, $a/t = 0.32, 0.5, 0.7$, and 0.9)	19
6	Tabulated Values of the Normalized Stress-Intensity Factors Along Straight Crack Fronts Located in Region III ($a/t = 1.1, 1.2, 1.4, 1.6$, and 2.0)	20

EXECUTIVE SUMMARY

Small cracks developing from rivet holes in lap joints of fuselage structure have been an issue of concern over the past decade. Stress-intensity factor solutions required to assess the structural integrity of such configurations are lacking. To address this need, the domain integral method was used in this research to obtain the mode I, normalized stress-intensity factor distributions for cracks emanating from a centrally located countersunk rivet hole in a square plate subjected to remote tension. Particular attention was focused on short cracks with an elliptical shape that have not propagated through the thickness. For these short cracks, the normalized stress-intensity factor distribution depended on the shape and size of the crack. Analysis was also conducted on long through-the-thickness cracks with a straight front for which the normalized stress-intensity factors were uniform.

1. INTRODUCTION.

During the last two decades, various methods, such as the finite element method (with or without singularity elements) and the boundary integral equation method, have been employed to obtain stress-intensity factor distributions for surface cracks and corner cracks in plates, see, Raju and Newman [1] and Newman and Raju [2]. Another well established and particularly useful method for evaluating fracture parameters is the domain integral method in which the crack tip integral is recast as an integral over a finite domain surrounding the crack tip. The calculation of the crack tip parameters of interest can then be carried out in a straightforward post processing step in the finite element method. The domain integral method has been employed by Shih, Moran, and Nakamura [3] to evaluate the energy release rate along a three-dimensional crack front in a thermally stressed body and has been used by Nikishkov and Atluri [4] to evaluate the mixed-mode stress-intensity factors along an arbitrary three-dimensional crack.

In this report, we employ the domain integral method to obtain the mode I stress-intensity factor distributions for elliptical and straight cracks emanating from a centrally located countersunk rivet hole in a square plate subjected to remote tension. Particular attention is focused on short cracks—cracks that have not propagated beyond the edge of the countersink. Related work on elliptical cracks emanating at various locations from countersunk rivet holes has been recently carried out by Tan et al. [5] using the finite element alternating method. In the finite element alternating method, two solution procedures are required to obtain the stress-intensity factor distribution for a particular crack geometry in a finite body. First, the stress distribution in the uncracked solid is obtained by the finite element method. Second, the analytical solution for an embedded elliptical crack in an infinite solid is combined with the finite element solution. The resulting nonzero tractions on external surfaces and crack faces are then canceled in an iterative manner using suitable polynomial inverse functions and finite element solutions on the uncracked geometry.

Although fracture parameters can be obtained very accurately using the domain integral method for arbitrary three-dimensional geometries, the method is expensive in terms of the time required to generate a mesh, in-core storage requirements for large three-dimensional calculations, and solution time. Mesh generation is particularly time consuming due to the difficulties associated with constructing a mesh which accurately captures the singular nature of the stress field in the vicinity of the crack front and near stress concentrations. On the other hand, the finite element alternating method is less time consuming because only the uncracked geometry needs to be meshed. The present work will compare stress-intensity factor solutions for a rivet hole geometry with solutions obtained by other techniques or by other finite element discretizations.

We define the geometry of the problem in section 2 and present a general three-dimensional domain integral formulation and associated finite element implementation in section 3. The numerical results are presented in section 4, followed by a summary and some concluding remarks in section 5.

2. PROBLEM FORMULATION.

We consider the problem of a square plate with a centrally located countersunk rivet hole subjected to uniform tensile loading as shown in figure 1. The dimensions of the plate are

$$W/H = 1.0$$

$$W/R = 9.6$$

and the remote applied stress is taken to be unity $\sigma_0 = 1$ MPa. A cross-sectional view illustrating the characteristic dimensions of the rivet hole is shown in figure 2. We choose a Cartesian coordinate system such that the load acts in the y direction as shown. The countersink angle ϕ and the ratios h/t and R/t are taken to be that of a standard rivet configuration ($\phi = 50^\circ$, $h/t = 0.2$, $R/t = 1.954$). These dimensions are also consistent with the dimensions of the sample used in a recent experimental study by Fadrakas and Fine [6]. The plate material is assumed to be linearly elastic and isotropic. The elastic constants of the plate are taken to be that of Alclad 2024-T3 aluminum with a Young's modulus of 73 GPa and Poisson's ratio $\nu = 0.3$.

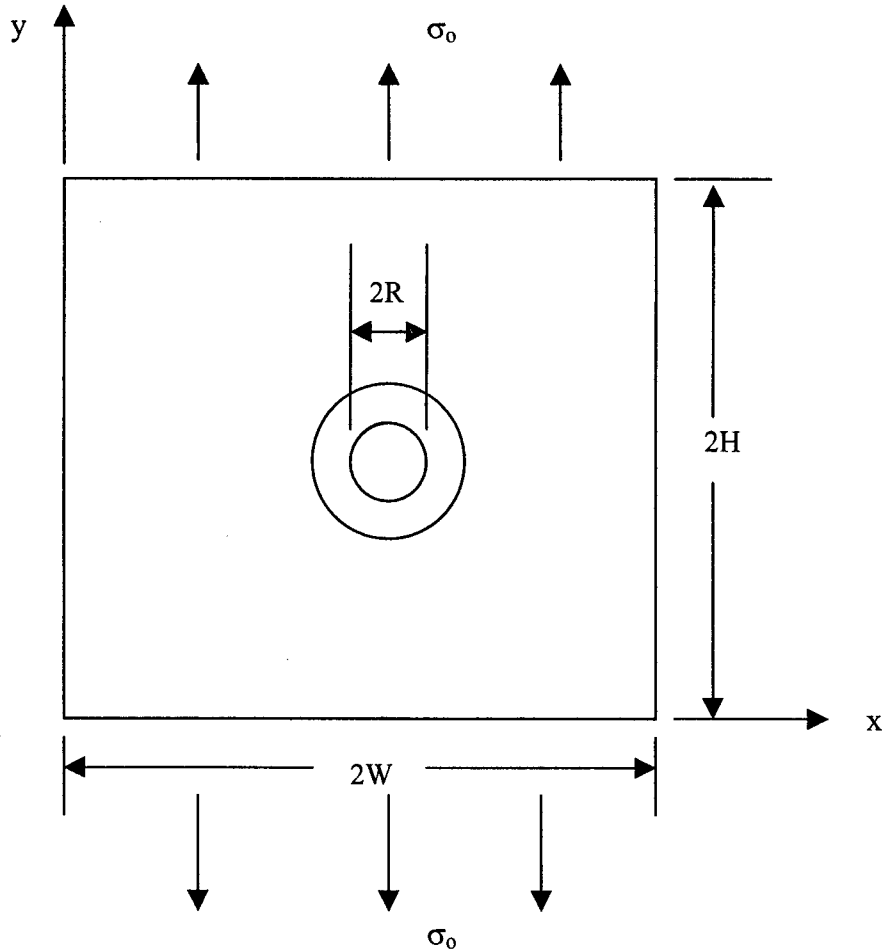


FIGURE 1. SPECIMEN GEOMETRY ($W/H=1.0$, $W/R=9.6$, $\sigma_0=1$ MPa)

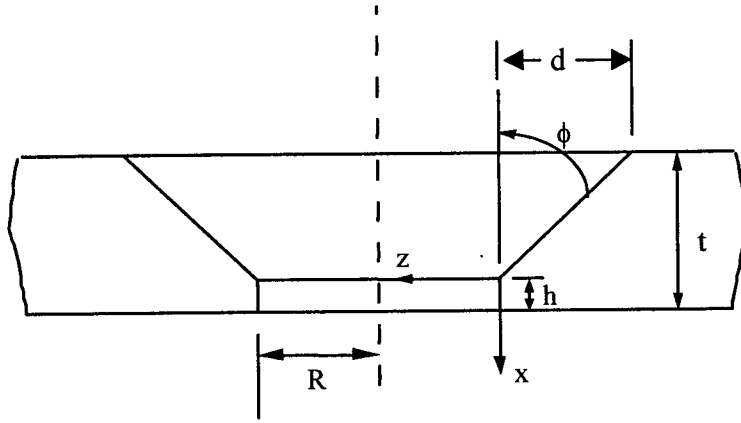


FIGURE 2. SPECIMEN GEOMETRY ($h/t=0.2$, $\phi=50^\circ$, $R/t=1.954$)

In the present analysis, cracks with elliptical crack fronts of various shapes and lengths were assumed to initiate at the intersection between the countersunk and straight shank portion of the rivet hole as shown in figure 3. We define three crack growth regions as I, II, and III respectively as shown in the figure. The extent of the crack growth regions is defined as follows:

$$\begin{aligned} \text{Region I} & \quad 0 < a < h \\ \text{Region II} & \quad h < a < d \\ \text{Region III} & \quad d < a \end{aligned}$$

where a is the major or minor axis of the elliptical crack measured from the origin of the coordinate system in figure 2, d is the dimension from the origin to the end of the countersink, and h is the height of the knee in the countersink. The crack front is assumed to be elliptical in regions I and II with various shapes defined by the ratio a/c . The crack front is assumed to be straight in region III.

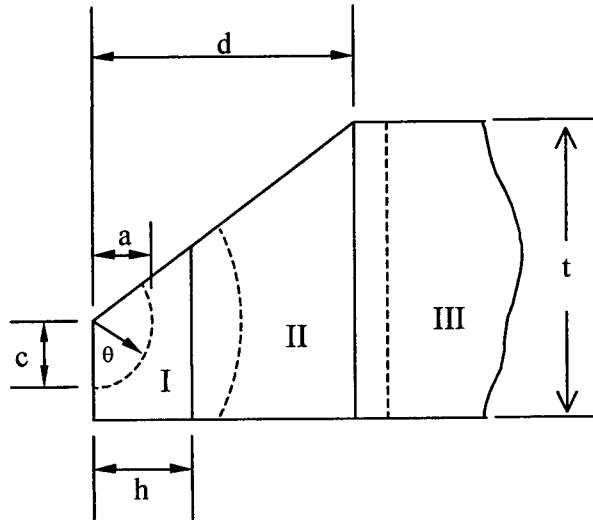


FIGURE 3. THE THREE CRACK GROWTH REGIONS I, II, AND III

3. DOMAIN INTEGRAL METHOD.

In this section we outline the formulation and finite element implementation of the domain integral method. Consider a curved crack front lying in the $x_1' - x_3$ plane as shown in figure 4. We denote by s and $v(s)$ a point lying on the crack front and the in-plane unit outward normal vector at s , respectively. The pointwise energy release rate $J(s)$ is given by

$$J(s) = v_k(s) \lim_{\Gamma \rightarrow 0} \int_{\Gamma(s)} [W\delta_{ik} - \sigma_{ij}u_{j,k}]m_i d\Gamma \quad (1)$$

where W is the strain energy density, σ_{ij} and $u_{j,k}$ are the Cartesian components of the stress and displacement, and m_i are the components of the unit outward normal to the curve Γ lying in the $x_1' - x_2$ plane which passes through point s as shown in figure 5. The energy released when a finite segment, L_c , of the crack front advances an amount $\Delta a l_k(s)$ is given by

$$\bar{J}\Delta a = \Delta a \int_{L_c} J(s)v_k(s)l_k(s)ds \quad (2)$$

where $l_k(s)$ are the components of an arbitrary unit vector at s lying in the plane of the crack.

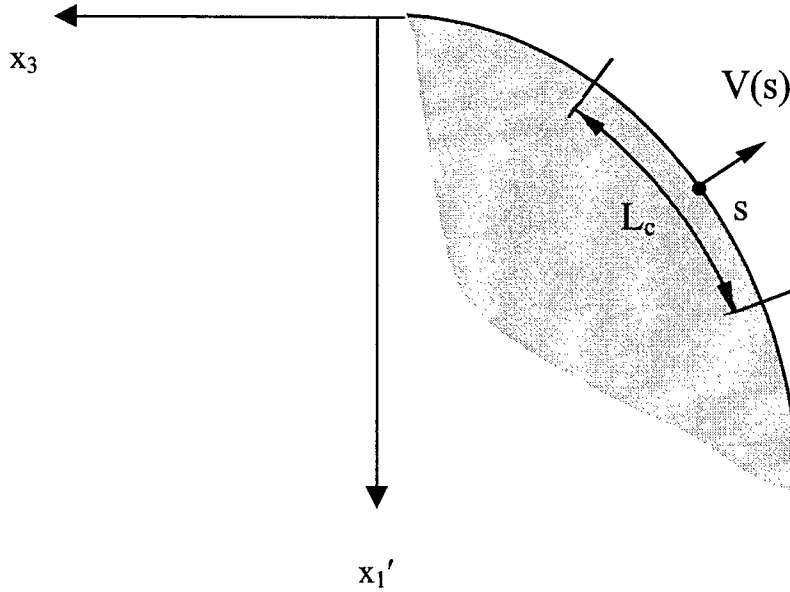


FIGURE 4. A POINT s LYING ON A CURVED CRACK FRONT

By substituting equation 1 into equation 2, we obtain the following expression for \bar{J} :

$$\bar{J} = \lim_{\Gamma \rightarrow 0} \int_{\Gamma_t} [W\delta_{ik} - \sigma_{ij}u_{j,k}]l_k m_i dA \quad (3)$$

where Γ_t is a tubular surface surrounding the crack segment L_c .

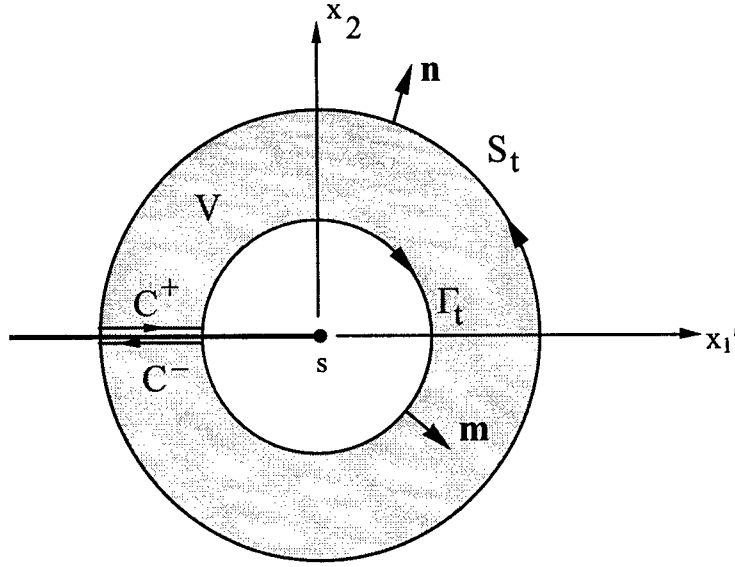


FIGURE 5. THE DOMAIN V ENCLOSED BY THE TUBULAR SURFACES S_t AND Γ_t

In order to obtain a domain integral, we introduce another tubular surface S_t which surrounds Γ_t as shown in two dimensions in figure 5. In the figure, we denote by \mathbf{n} the unit outward normal to the surface S_t and define V to be the volume enclosed by the surfaces Γ_t , S_t , and the upper and lower crack surfaces C^+ and C^- along the crack segment. In the absence of body forces, thermal strains, and crack face tractions, the bracketed quantity in equations 1 and 3 is divergence free. Hence, letting

$$H_{ki} = \sigma_{ij} u_{j,k} - W \delta_{ik} \quad (4)$$

it follows that

$$H_{ki,i} = 0 \quad \text{in } V \quad (5)$$

We now define a vector-valued test function q_k as follows:

$$q_k = \begin{cases} l_k & \text{on } \Gamma_t \\ 0 & \text{on } S_t \end{cases} \quad (6)$$

Assuming q_k is sufficiently smooth to justify the following manipulations, we take the inner product of q_k with the left-hand side of equation 5 to obtain

$$\int_V H_{ki,i} q_k dV = 0 \quad (7)$$

Next, we employ the divergence theorem and the definition of the test function (equation 6) to obtain

$$\int_{\Gamma_t} H_{ki} l_k n_i dA = \int_V H_{ki} q_{k,i} dV \quad (8)$$

Noting that $n_i = -m_i$ on Γ_t , we obtain an expression for \bar{J} in terms of the volume integral

$$\bar{J} = \int_V H_{ki} q_{k,i} dV \quad (9)$$

Finally, if we assume that $J(s)$ is constant over the crack segment L_c , $J(s)$ can be taken outside the integral in (2) and we obtain a simple expression for $J(s)$ in terms of \bar{J}

$$J(s) = \frac{\bar{J}}{\int_{L_c} l_k \nu_k ds} \quad (10)$$

In order to illustrate the numerical evaluation of equation 10, we consider a schematic discretization of the volume V surrounding the crack segment into 32 eight-node brick elements as shown in figures 6 and 7 (more refined meshes are used in the actual calculations). A cross section of the schematic finite element mesh perpendicular to the crack plane passing through node M on the crack surface is illustrated in figure 6. A view of the mesh cross section lying in the plane of the crack and passing through M is shown in figure 7. Consistent with a standard isoparametric finite element implementation, we define the test function q_k within an element in V using the trilinear finite element shape functions, i.e.,

$$q_k = \sum_{a=1}^8 N_a Q_k^a \quad (11)$$

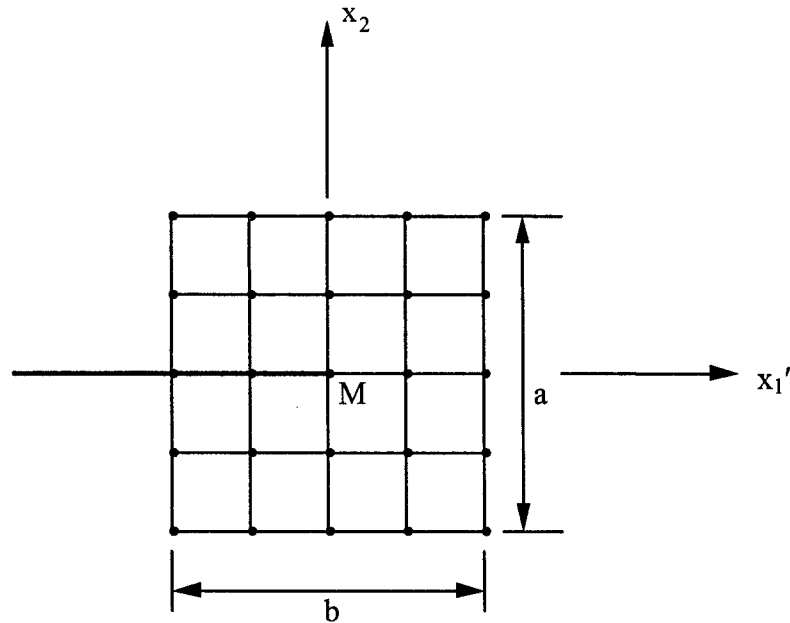


FIGURE 6. CROSS SECTION OF A FINITE ELEMENT MESH PERPENDICULAR TO THE CRACK PLANE PASSING THROUGH NODE M

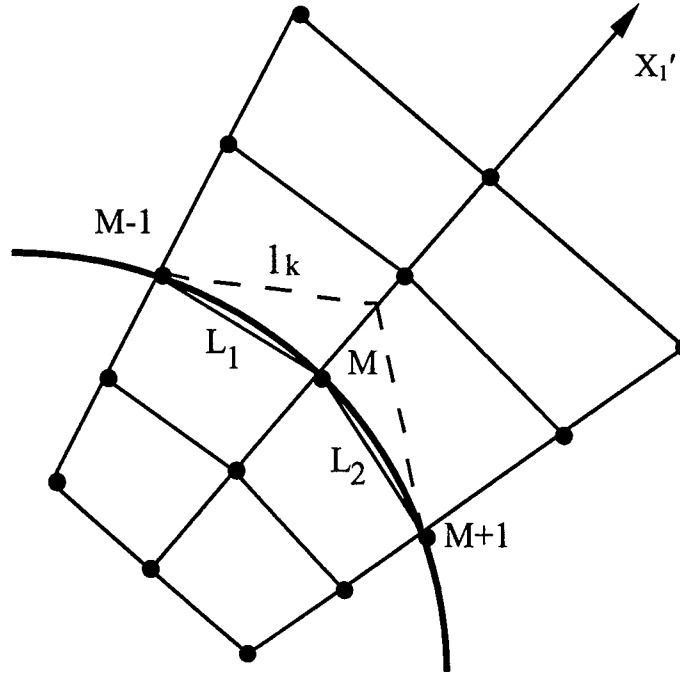


FIGURE 7. CROSS SECTION OF A FINITE ELEMENT MESH PARALLEL TO THE CRACK PLANE AND PASSING THROUGH NODE M

In equation 11, Q_k^a are the discrete nodal values of the test function. In the present analysis we have chosen the nodal values such that

$$Q_k^a = \begin{cases} v_k^M & \text{if } x_3^a = 0 \text{ and } |x_2^a| < b \text{ and } |x_1^a| < a \\ 0 & \text{otherwise} \end{cases} \quad (12)$$

In other words, the nodal value Q_k^a is defined to be equal to the in-plane unit normal vector v_k^M at node M if the node lies in the plane perpendicular to the crack plane which passes through node M and does not lie on the boundary of V. In the present implementation, we have defined the volume V to be rectangular with height b and width a as shown in figure 6.

The discrete form of the integral (9) is then written as

$$\bar{J}^M = \sum_{e \in V} \{ \int_{\Omega_e} H_{ki} q_{k,i} d\Omega \} \quad (13)$$

where

$$q_{k,i} = \sum_{a=1}^8 N_{a,i} Q_k^a \quad (14)$$

In the present analysis, the integration (13) was carried out using 2x2x2 Gaussian quadrature.

In order to evaluate the integral in the denominator of equation 10, we assume that the energy release rate is constant over the crack segment L_c and define the vector l_k along the crack segment as follows:

$$l_k^M = \begin{cases} v_k^M & \text{at node M} \\ 0 & \text{at all other nodes on crack front} \end{cases} \quad (15)$$

By taking l_k to vary linearly between the nodes $M - 1$, M , and $M + 1$ as shown in figure 7, we obtain the pointwise energy release rate at node M

$$J^M = \frac{2\bar{J}^M}{L_1 + L_2} \quad (16)$$

where L_1 and L_2 are the lengths of the element edges containing nodes $M - 1$, M , and $M + 1$.

A typical finite element mesh used in the numerical calculations is shown in figure 8. Due to symmetry, only one quarter of the plate was analyzed. The mesh shown in the figure is made up of 5312 eight-node brick elements (with 6,497 nodes and 19,491 degrees of freedom) and was employed to obtain the stress-intensity factor distribution along an elliptical crack front located in region I. A magnification of the mesh in the vicinity of the edge of the countersink is shown in figure 9. In order to construct the finite element domains necessary for the present domain integral approach, a two-dimensional rectangular mesh composed of 51 elements was swept around the elliptical crack front to create the three-dimensional mesh as shown in figure 10.

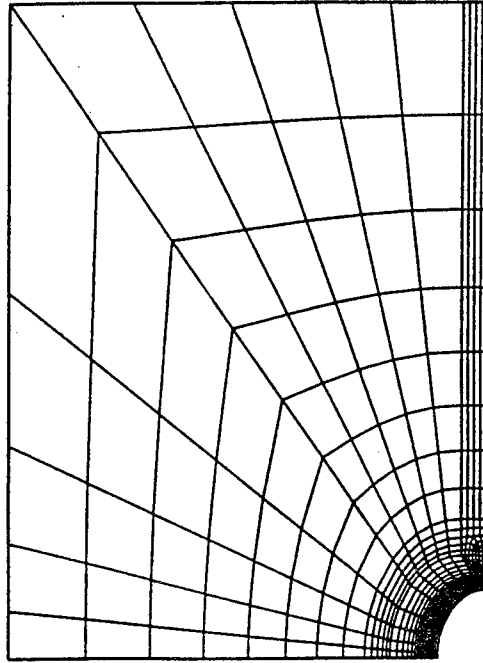


FIGURE 8. THE FINITE ELEMENT MESH FOR THE CASE OF AN ELLIPTICAL CRACK LOCATED IN REGION I

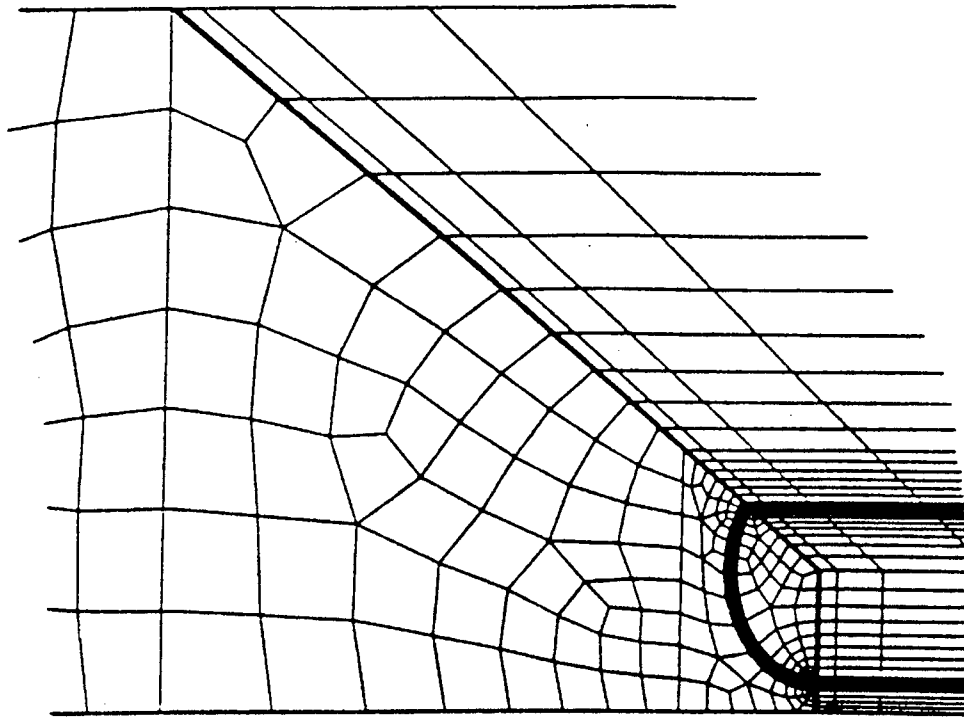


FIGURE 9. A MAGNIFICATION OF THE MESH NEAR THE INTERSECTION BETWEEN THE COUNTERSUNK AND STRAIGHT SHANK PORTION OF THE RIVET HOLE

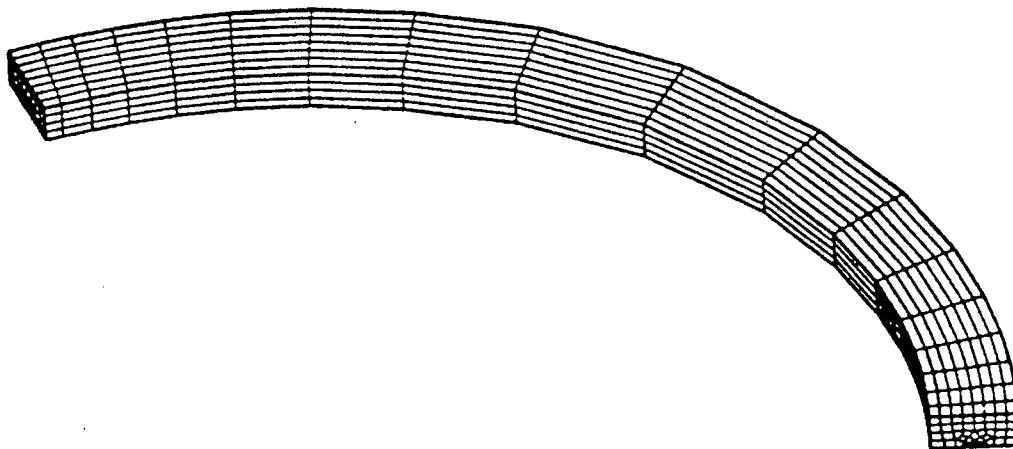


FIGURE 10. THE FINITE ELEMENT DOMAINS ALONG AN ELLIPTICAL CRACK FRONT

Before performing the numerical calculations, benchmark comparisons were carried out in order to validate the present three-dimensional domain integral implementation and to determine the

necessary mesh refinement. Stress-intensity factor distributions were obtained for both an embedded elliptical crack and a quarter elliptical corner crack in a rectangular plate. As reported in Gosz and Moran [7], excellent agreement was observed between the finite element/domain integral solutions and the benchmark solutions from the literature.

The meshes employed in the present calculations had between 18,000 and 21,000 degrees of freedom, and the calculations were performed on a Silicon Graphics R4000 workstation equipped with 192 megabytes of random access memory (RAM).

4. NUMERICAL RESULTS.

In all of the numerical calculations, the pointwise energy release rates $J(s)$ along the crack front were obtained by the domain integral method as described in the previous section. The mode I stress-intensity factors $K_I(s)$ at each point along the crack front were obtained using the plane strain relation

$$K_I(s) = \left\{ \frac{EJ(s)}{1 - \nu^2} \right\}^{1/2} \quad (17)$$

where E is Young's modulus and ν is Poisson's ratio. Although we recognize that the asymptotic field has a lower order singularity than $1/\sqrt{r}$ near intersections of the crack front and free surfaces, the extent of the boundary layer is known to be small and thus equation 1 was used throughout for the computation of K_I .

The mode I stress-intensity factor at a point along the crack front can be expressed in terms of the remote applied stress σ_o and a boundary correction factor F as

$$K_I(s) = F(a/c, a/t, \theta) \sigma_o \sqrt{\pi a Q} \quad (18)$$

where the parameter Q is the square of the complete elliptical integral of the second kind. In this report, Q was approximated by the formula given by Raju and Newman [1],

$$Q = 1 + 1.464 \left(\frac{a}{c} \right)^{1.65} \quad \frac{a}{c} \leq 1 \quad (19)$$

Boundary correction factors F for elliptical cracks located in region I are plotted versus physical angle θ in figures 11-13. In figure 11, the boundary correction factors are plotted along the crack front for $a/c = 0.4$ for three different ratios of c/h ($c/h = 0.4, 0.6$, and 0.8). Note that c is the characteristic dimension of the ellipse as shown in figure 3, and h is the height of the straight shank portion of the rivet hole. The boundary correction factors for the case where $a/c = 0.8$ and $a/c = 1.0$ are plotted versus physical angle for four different ratios of c/h ($c/h = 0.2, 0.4, 0.6$, and 0.8) in figures 12 and 13, respectively. As shown in the figures, the boundary correction factor distributions depend heavily on the ratio a/c , but the distributions for each ratio of a/c do not significantly differ for different values of c/h .

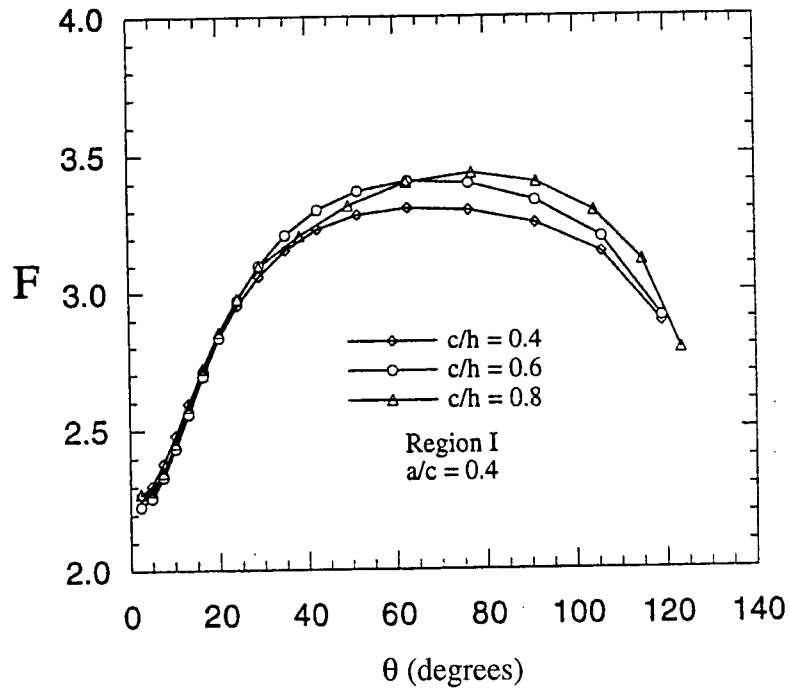


FIGURE 11. BOUNDARY CORRECTION FACTORS F VERSUS PHYSICAL ANGLE θ FOR ELLIPTICAL CRACKS LOCATED IN REGION I ($a/c = 0.4$, $c/h = 0.4$, 0.6 , AND 0.8)

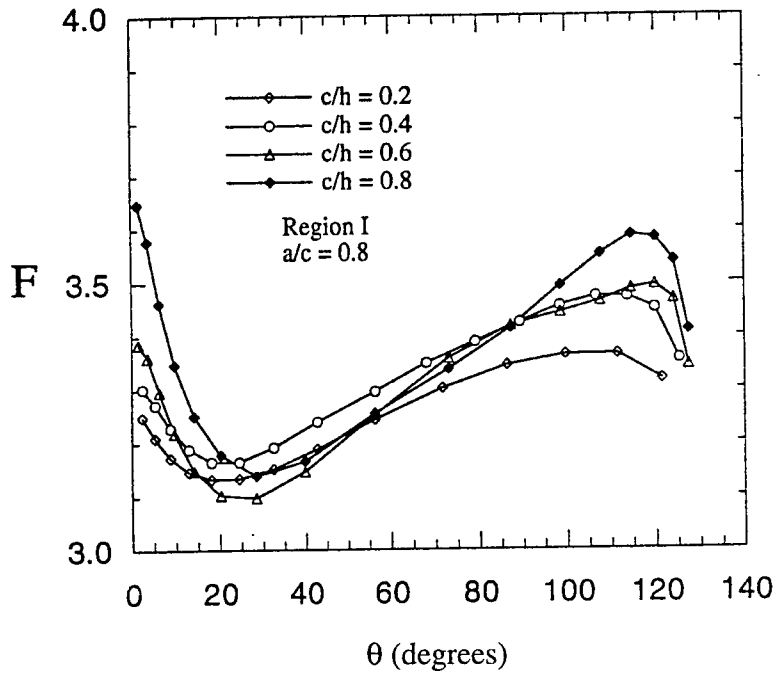


FIGURE 12. BOUNDARY CORRECTION FACTORS F VERSUS PHYSICAL ANGLE θ FOR ELLIPTICAL CRACKS LOCATED IN REGION I ($a/c = 0.8$, $c/h = 0.2$, 0.4 , 0.6 , AND 0.8)

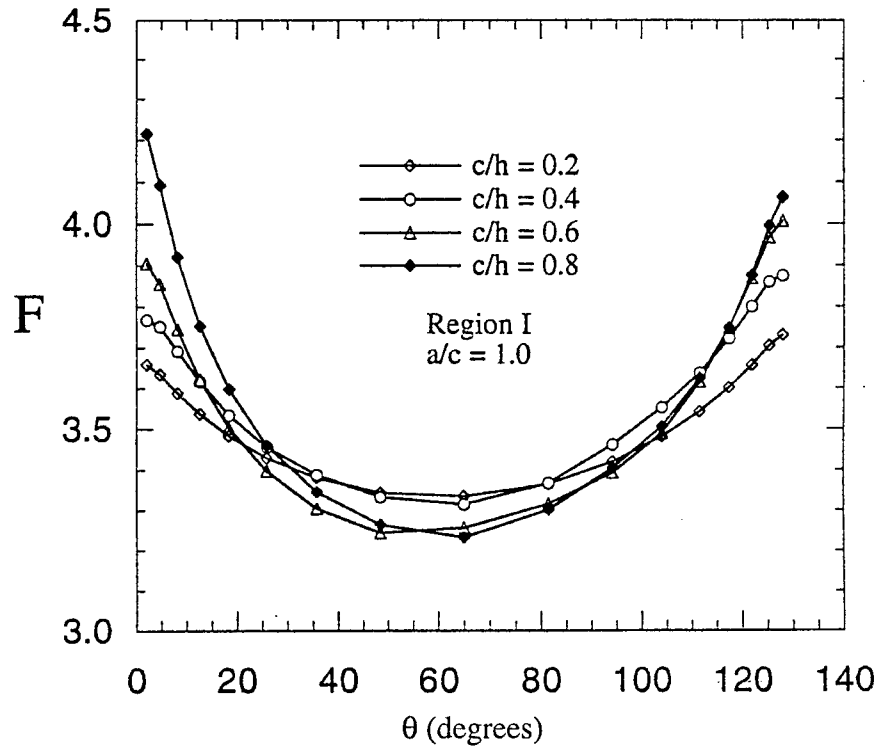


FIGURE 13. BOUNDARY CORRECTION FACTORS F VERSUS PHYSICAL ANGLE θ FOR ELLIPTICAL CRACKS LOCATED IN REGION I ($a/c = 1.0$, $c/h = 0.2$, 0.4 , 0.6 , AND 0.8)

The boundary correction factors for elliptical cracks located in region II are plotted versus physical angle in figures 14 and 15. In figure 14, the boundary correction factors are plotted for five different ratios of a/t ($a/t = 0.16$, 0.32 , 0.5 , 0.7 , and 0.9) for the aspect ratio $a/c = 0.4$. The distributions for $a/c = 0.8$ and $a/t = 0.32$, 0.5 , 0.7 , and 0.9 are shown in figure 15. As shown in figure 14, the values of F tend to be relatively constant along the crack front until they drop off near the free edge where the crack front intersects the countersunk surface. As shown in figure 15, the values of F are highest at the intersection of the crack front with the bottom surface of the plate. We note that the boundary correction factors are significantly higher for smaller values of a/t within region II for both ratios of a/c considered.

The crack fronts are assumed to be straight in region III as depicted in figure 3. The mode I stress-intensity factors normalized with respect to the remote applied stress and the length $a' = a + R$ are plotted versus a normalized length x/t for five values of a/t ($a/t = 1.1$, 1.2 , 1.4 , 1.6 , and 2.0) in figure 16. As shown in the figure, for the largest value of a/t considered ($a/t = 2.0$), the normalized stress-intensity factors are relatively constant through the thickness of the plate except near the intersections of the crack front with the top and bottom surfaces of the plate.

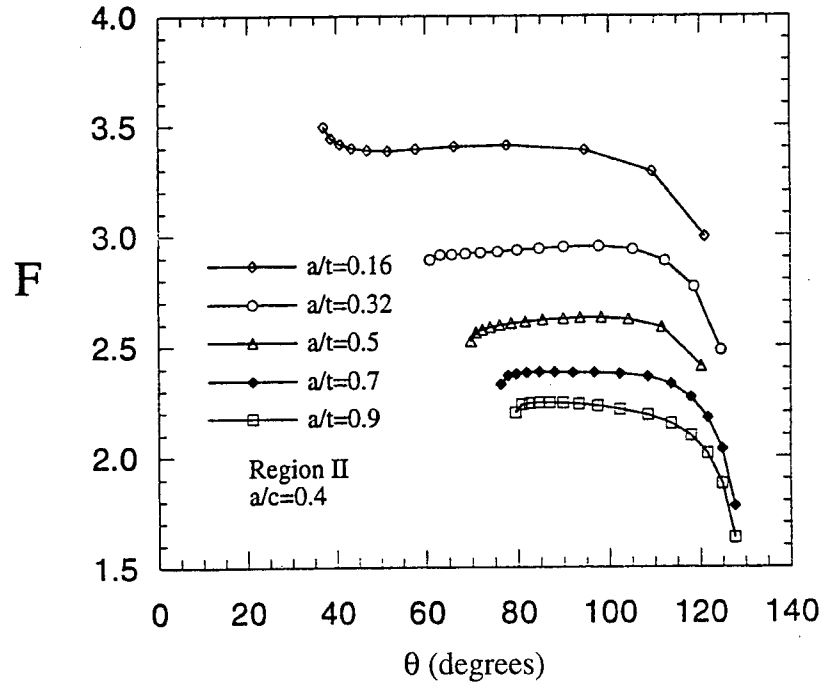


FIGURE 14. BOUNDARY CORRECTION FACTORS F VERSUS PHYSICAL ANGLE θ FOR ELLIPTICAL CRACKS LOCATED IN REGION II ($a/c = 0.4$, $a/t = 0.16, 0.32, 0.5, 0.7$, AND 0.9)

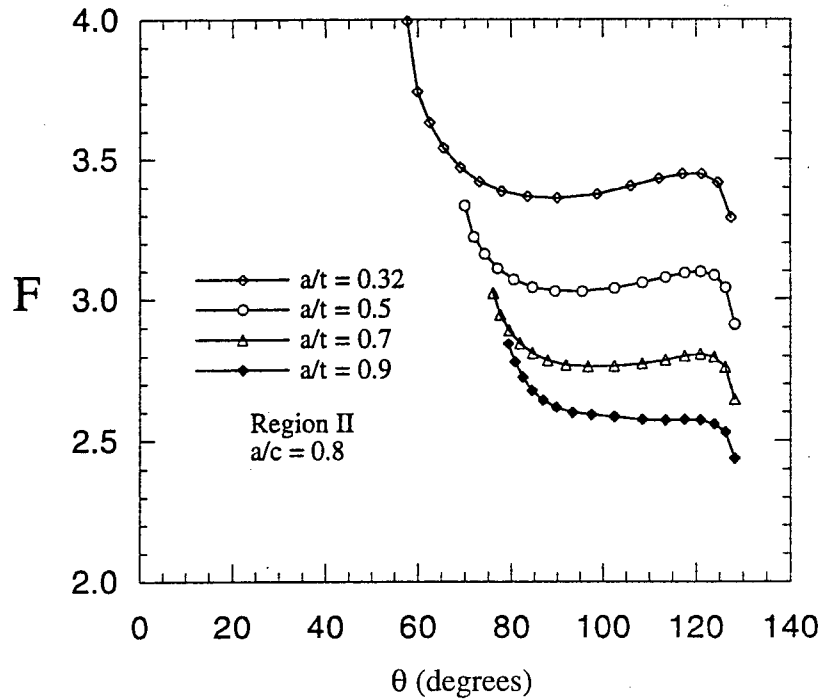


FIGURE 15. BOUNDARY CORRECTION FACTORS F VERSUS PHYSICAL ANGLE θ FOR ELLIPTICAL CRACKS LOCATED IN REGION II ($a/c = 0.8$, $a/t = 0.32, 0.5, 0.7$, AND 0.9)

To compare the present three-dimensional results with corresponding two-dimensional results obtained from the literature, we have also plotted in figure 16 the plane strain/stress value obtained by Fuhring [8] for a two-dimensional plate of width W having a centrally located hole of radius R for the largest value of a considered (shown as the dashed-dot line in the figure). It is interesting to note that the three-dimensional results obtained for the case where $a/t = 2.0$ when the crack front is significantly beyond the edge of the countersink are higher than the two-dimensional value (approximately 12 percent higher).

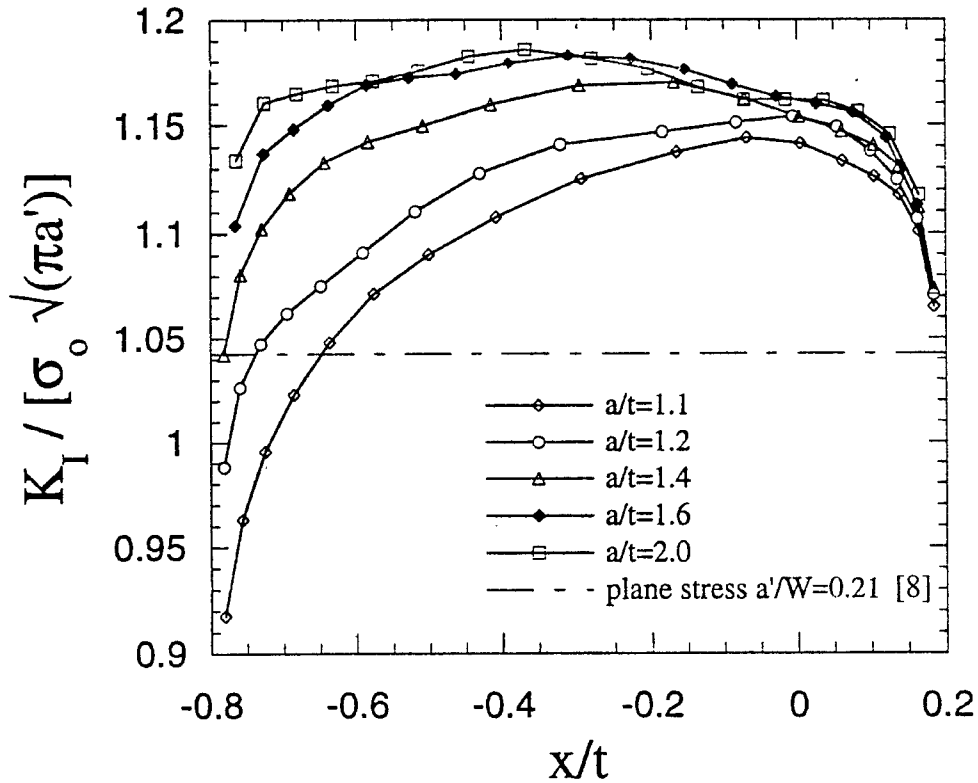


FIGURE 16. NORMALIZED MODE I STRESS-INTENSITY FACTORS ALONG STRAIGHT CRACK FRONTS IN REGION III ($a/t = 1.1, 1.2, 1.4, 1.6$, AND 2.0)

The numerical data for the plots shown in figures 11 to 16 are given in tables 1 to 6.

TABLE 1. TABULATED VALUES OF THE BOUNDARY CORRECTION FACTORS F VERSUS PHYSICAL ANGLE θ FOR ELLIPTICAL CRACKS LOCATED IN REGION I ($a/c = 0.4$, $c/h = 0.4, 0.6$, AND 0.8)

$c/h=0.4$	
θ	F
2.4198	2.2710
4.8853	2.3030
7.4453	2.3813
10.155	2.4819
13.082	2.5947
16.309	2.7140
19.946	2.8347
24.137	2.9515
29.082	3.0595
35.049	3.1541
42.393	3.2300
51.532	3.2819
62.834	3.3058
76.300	3.2983
91.154	3.2500
105.88	3.1434
119.04	2.8852

$c/h=0.6$	
θ	F
2.4198	2.2303
4.8853	2.2596
7.4453	2.3336
10.155	2.4362
13.082	2.5585
16.309	2.6933
19.946	2.8333
24.137	2.9713
29.082	3.0994
35.049	3.2106
42.393	3.3008
51.532	3.3681
62.834	3.4040
76.300	3.3963
91.154	3.3332
105.88	3.1999
119.04	2.9057

$c/h=0.8$	
θ	F
2.4198	2.2753
4.8853	2.2872
7.4453	2.3510
10.155	2.4547
13.082	2.5835
16.309	2.7209
19.946	2.8545
24.137	2.9769
29.082	3.0955
38.299	3.2070
49.457	3.3158
62.605	3.3988
77.057	3.4330
91.402	3.3978
104.23	3.2933
114.86	3.1139
123.33	2.7863

TABLE 2. TABULATED VALUES OF THE BOUNDARY CORRECTION FACTORS F VERSUS PHYSICAL ANGLE θ FOR ELLIPTICAL CRACKS LOCATED IN REGION I ($a/c = 0.8$, $c/h = 0.2, 0.4, 0.6$, AND 0.8)

$c/h=0.2$	
θ	F
2.3831	3.2484
5.2493	3.2098
8.7088	3.1726
12.908	3.1464
18.047	3.1329
24.414	3.1341
32.435	3.1519
42.756	3.1885
56.320	3.2431
71.669	3.3020
86.316	3.3446
99.665	3.3640
111.39	3.3656
121.45	3.3180

$c/h=0.4$	
θ	F
2.3831	3.3017
5.2493	3.2717
8.7088	3.2281
12.908	3.1890
18.047	3.1651
24.414	3.1651
32.435	3.1915
42.756	3.2389
56.320	3.2959
67.951	3.3490
78.982	3.3890
89.171	3.4249
98.363	3.4560
106.51	3.4733
113.65	3.4724
119.88	3.4508
125.29	3.3554

$c/h=0.6$	
θ	F
1.5479	3.3861
3.5622	3.3609
6.1887	3.2955
9.6257	3.2187
14.153	3.1486
20.183	3.1037
28.366	3.0985
39.792	3.1469
56.320	3.2521
72.985	3.3582
87.113	3.4194
98.536	3.4433
107.52	3.4644
114.50	3.4873
119.92	3.4947
124.13	3.4681
127.42	3.3443

$c/h=0.8$	
θ	F
1.5479	3.6473
3.5622	3.5778
6.1887	3.4623
9.6257	3.3471
14.153	3.2503
20.183	3.1779
28.366	3.1393
39.792	3.1657
56.320	3.2548
72.985	3.3379
87.113	3.4145
98.536	3.4936
107.52	3.5525
114.50	3.5873
119.92	3.5823
124.13	3.5396
127.42	3.4093

TABLE 3. TABULATED VALUES OF THE BOUNDARY CORRECTION FACTORS F VERSUS PHYSICAL ANGLE θ FOR ELLIPTICAL CRACKS LOCATED IN REGION I ($a/c = 1.0$, $c/h = 0.2, 0.4, 0.6$, AND 0.8)

$c/h=0.2$	
θ	F
2.0303	3.6581
4.6697	3.6342
8.1009	3.5887
12.561	3.5378
18.360	3.4837
25.899	3.4295
35.698	3.3804
48.438	3.3430
65.000	3.3348
81.522	3.3642
94.244	3.4192
104.04	3.4804
111.58	3.5420
117.39	3.6012
121.86	3.6561
125.31	3.7042
127.96	3.7299

$c/h=0.4$	
θ	F
2.0303	3.7680
4.6697	3.7519
8.1009	3.6925
12.561	3.6166
18.360	3.5345
25.899	3.4559
35.698	3.3880
48.438	3.3326
65.000	3.3145
81.522	3.3665
94.244	3.4616
104.04	3.5521
111.58	3.6372
117.39	3.7218
121.86	3.7999
125.31	3.8594
127.96	3.8744

$c/h=0.6$	
θ	F
2.0303	3.9051
4.6697	3.8541
8.1009	3.7450
12.561	3.6215
18.360	3.5032
25.899	3.3970
35.698	3.3042
48.438	3.2436
65.000	3.2560
81.522	3.3155
94.244	3.3915
104.04	3.4884
111.58	3.6149
117.39	3.7462
121.86	3.8675
125.31	3.9670
127.96	4.0070

$c/h=0.8$	
θ	F
2.0303	4.2155
4.6697	4.0924
8.1009	3.9201
12.561	3.7531
18.360	3.5984
25.899	3.4601
35.698	3.3456
48.438	3.2638
65.000	3.2326
81.522	3.3011
94.244	3.4032
104.04	3.5057
111.58	3.6246
117.39	3.7475
121.86	3.8752
125.31	3.9953
127.96	4.0634

TABLE 4. TABULATED VALUES OF THE BOUNDARY CORRECTION FACTORS F VERSUS PHYSICAL ANGLE θ FOR ELLIPTICAL CRACKS LOCATED IN REGION II ($a/c = 0.8$, $a/t = 0.16, 0.32, 0.5, 0.7$, AND 0.9)

$a/t=0.16$	
θ	F
37.092	3.4958
38.746	3.4429
40.843	3.4164
43.532	3.3985
47.029	3.3885
51.650	3.3873
57.853	3.3941
66.278	3.4052
77.662	3.4111
94.614	3.3897
109.39	3.2904
121.09	2.9949

$a/t=0.32$	
θ	F
60.863	2.8917
63.101	2.9136
65.649	2.9163
68.550	2.9195
71.854	2.9231
75.611	2.9281
79.867	2.9348
84.658	2.9422
90.000	2.9492
97.692	2.9519
105.16	2.9374
112.21	2.8862
118.73	2.7689
124.66	2.4829

$a/t=0.5$	
θ	F
69.678	2.5243
70.832	2.5635
72.235	2.5759
73.943	2.5867
76.025	2.5959
78.564	2.6042
81.662	2.6120
85.433	2.6193
90.000	2.6252
93.632	2.6295
98.314	2.6299
104.26	2.6210
111.60	2.5860
120.29	2.4103

$a/t=0.7$	
θ	F
76.268	2.3297
77.804	2.3681
79.666	2.3759
81.926	2.3822
84.664	2.3850
87.977	2.3836
91.966	2.3817
96.728	2.3805
102.34	2.3758
108.44	2.3626
113.65	2.3305
118.07	2.2686
121.81	2.1749
124.99	2.0342
127.69	1.7791

$a/t=0.9$	
θ	F
79.491	2.2005
80.857	2.2372
82.508	2.2426
84.503	2.2445
86.912	2.2445
89.814	2.2430
93.296	2.2381
97.446	2.2288
102.34	2.2132
108.44	2.1883
113.65	2.1489
118.07	2.0948
121.81	2.0138
124.99	1.8794
127.69	1.6325

TABLE 5. TABULATED VALUES OF THE BOUNDARY CORRECTION FACTORS F VERSUS PHYSICAL ANGLE θ FOR ELLIPTICAL CRACKS LOCATED IN REGION II ($a/c = 0.8$, $a/t = 0.32, 0.5, 0.7$, AND 0.9)

$a/t=0.32$	
θ	F
57.705	3.9931
59.911	3.7430
62.486	3.6313
65.492	3.5400
69.007	3.4701
73.116	3.4194
77.917	3.3859
83.513	3.3673
90.000	3.3615
98.706	3.3747
106.00	3.4031
112.06	3.4298
117.09	3.4472
121.26	3.4475
124.72	3.4153
127.60	3.2911

$a/t=0.5$	
θ	F
70.001	3.3344
71.912	3.2227
74.224	3.1616
77.022	3.1101
80.409	3.0697
84.504	3.0423
89.444	3.0287
95.373	3.0278
102.43	3.0392
108.42	3.0593
113.41	3.0784
117.56	3.0930
121.01	3.0982
123.89	3.0858
126.30	3.0417
128.31	2.9107

$a/t=0.7$	
θ	F
76.042	3.0215
77.622	2.9441
79.526	2.8887
81.822	2.8437
84.589	2.8100
87.921	2.7848
91.926	2.7687
96.721	2.7621
102.43	2.7638
108.42	2.7727
113.41	2.7865
117.56	2.8004
121.01	2.8066
123.89	2.7968
126.30	2.7608
128.31	2.6466

$a/t=0.9$	
θ	F
79.387	2.8432
80.776	2.7791
82.447	2.7243
84.459	2.6773
86.879	2.6422
89.788	2.6167
93.279	2.5995
97.456	2.5908
102.43	2.5840
108.42	2.5737
113.41	2.5716
117.56	2.5740
121.01	2.5712
123.89	2.5575
126.30	2.5294
128.31	2.4373

TABLE 6. TABULATED VALUES OF THE NORMALIZED STRESS-INTENSITY FACTORS ALONG STRAIGHT CRACK FRONTS LOCATED IN REGION III ($a/t = 1.1, 1.2, 1.4, 1.6, \text{ AND } 2.0$). THE VALUES WERE OBTAINED FOR A REMOTE APPLIED STRESS OF UNITY.

$a/t=1.1$	
x/t	$K_I / \sqrt{\pi a'}$
0.184	1.065
0.164	1.101
0.138	1.118
0.104	1.126
0.061	1.133
0.004	1.141
-0.069	1.144
-0.165	1.138
-0.295	1.125
-0.408	1.107
-0.500	1.090
-0.576	1.071
-0.637	1.048
-0.686	1.023
-0.725	0.996
-0.756	0.963
-0.781	0.918

$a/t=1.2$	
x/t	$K_I / \sqrt{\pi a'}$
0.184	1.071
0.162	1.107
0.135	1.125
0.099	1.138
0.053	1.149
-0.006	1.154
-0.083	1.151
-0.185	1.147
-0.322	1.141
-0.431	1.128
-0.520	1.110
-0.591	1.091
-0.649	1.075
-0.695	1.062
-0.731	1.047
-0.760	1.026
-0.782	0.988

$a/t=1.4$	
x/t	$K_I / \sqrt{\pi a'}$
0.184	1.074
0.164	1.112
0.138	1.131
0.104	1.141
0.060	1.147
0.003	1.154
-0.072	1.162
-0.169	1.170
-0.298	1.169
-0.415	1.160
-0.509	1.150
-0.584	1.142
-0.644	1.133
-0.692	1.119
-0.730	1.102
-0.759	1.081
-0.782	1.042

$a/t=1.6$	
x/t	$K_I / \sqrt{\pi a'}$
0.162	1.113
0.121	1.144
0.076	1.156
0.026	1.160
-0.029	1.163
-0.089	1.169
-0.155	1.176
-0.229	1.181
-0.311	1.183
-0.391	1.179
-0.463	1.174
-0.528	1.172
-0.586	1.169
-0.638	1.159
-0.686	1.148
-0.728	1.137
-0.766	1.104

$a/t=2.0$	
x/t	$K_I / \sqrt{\pi a'}$
0.164	1.117
0.125	1.146
0.083	1.156
0.036	1.161
-0.016	1.162
-0.073	1.162
-0.135	1.168
-0.204	1.176
-0.281	1.181
-0.368	1.186
-0.445	1.182
-0.515	1.175
-0.577	1.171
-0.632	1.168
-0.681	1.165
-0.726	1.160
-0.765	1.134

5. SUMMARY AND CONCLUDING REMARKS.

Mode I stress-intensity factors along three-dimensional elliptical and straight crack fronts are obtained for the problem of a plate with a centrally located countersunk rivet hole subjected to uniform tensile loading. Attention is focused on short, symmetrically located cracks initiating at the intersection between the countersunk and straight shank portion of the rivet hole. The stress-intensity factors for cracks of various shapes and lengths are obtained by the domain integral method.

For cracks that have not propagated beyond the edge of the countersink (short cracks), we assumed the crack fronts to be elliptical and obtained stress-intensity factor distributions along crack fronts for a variety of shapes and sizes. For the shortest cracks considered (cracks that did not extend beyond the straight shank portion of the countersink), it was found that the boundary correction factors depend significantly on the shape of the elliptical front but do not depend heavily on the size of the crack. For elliptical crack fronts beyond the straight shank portion of the countersink but not yet through cracks, it was found that the dependence of the boundary correction factors on both crack size and shape was significant. For the case of straight crack fronts in region III, the normalized stress-intensity factors were relatively uniform through the thickness of the plate for the longest cracks considered (i.e., once the cracks had extended beyond the influence of the countersunk rivet hole) and the values were significantly higher than two-dimensional results for corresponding geometry obtained from the literature.

6. REFERENCES.

1. Raju, I. S. and Newman, J. C., Jr., 1979, "Stress-Intensity Factors for a Wide Range of Semi-Elliptical Surface Cracks in Finite Thickness Plates," *Engineering Fracture Mechanics*, Vol. 11, No. 4, pp. 817-829.
2. Newman, J. C., Jr. and Raju, I. S., 1983, "Stress-Intensity Factor Equations for Cracks in Three-Dimensional Finite Bodies," *Fracture Mechanics: Fourteenth Symposium—Volume I: Theory and Analysis, ASTM STP 791*, J. C. Lewis and G. Sines, Eds., American Society for Testing and Materials, pp. I-238-I-265.
3. Shih, C. F., Moran, B., and Nakamura, T., 1986, "Energy Release Rate Along a Three-Dimensional Crack Front in a Thermally Stressed Body," *International Journal of Fracture*, Vol. 30, pp. 79-102.
4. Nikishkov, G. P. and Atluri, S. N., 1987, "Calculation of Fracture Mechanics Parameters for an Arbitrary Three-Dimensional Crack by the "Equivalent Domain Integral Method," *International Journal of Numerical Methods in Engineering*, Vol. 24, pp. 1801-1821.
5. Tan, P. W., Bigelow, C. A., O'Donoghue, P. E., and Atluri, S. N., 1994, "Stress-Intensity Factor Solutions for Cracks at Countersunk Rivet Holes Under Uniaxial Tension," U.S. Department of Transportation Federal Aviation Administration, Report No. DOT/FAA/CT-93/68.
6. Fadragas, M. and Fine, M., 1993, "Tensile Fatigue Crack Initiation and Growth Database for Chamfered Rivet Holes in Alclad 2024-T3 Aluminum Alloy," U.S. Department of Transportation Federal Aviation Administration, Report Number DOT/FAA/AR-96/96.
7. Gosz, M. and Moran, B., 1994, "Stress-Intensity Factors Along Three-Dimensional Elliptical Crack Fronts," U.S. Department of Transportation Federal Aviation Administration, Report Number DOT/FAA/AR-96/97.
8. Fuhring, H., 1973, "Approximation Functions For K-Factors of Cracks in Notches," *International Journal of Fracture*, Vol. 9, pp. 328-329.